6-1-2005

CO Emission and Absorption toward V1647 Orionis (McNeil's Nebula)

Terrence W. Rettig
University of Notre Dame

Sean D. Brittain
Clemson University, sbritt@clemson.edu

Erika Gibb
University of Notre Dame

Theodore Simon
University of Hawaii

Craig Kulesa
University of Arizona

The Astrophysical Journal, 626:245–252, 2005 June 10

CO EMISSION AND ABSORPTION TOWARD V1647 ORIONIS (McNEIL'S NEBULA)

Terrence W. Rettig, Sean D. Brittain,[1] and Erika L. Gibb
Center for Astrophysics, University of Notre Dame, Notre Dame, IN 46556

Theodore Simon
Institute for Astronomy, University of Hawaii, 2680 Woodlawn Drive, Honolulu, HI 96822

and

Craig Kulesa
Steward Observatory, University of Arizona, 933 North Cherry Avenue, Tucson, AZ 85721
Received 2004 September 7; accepted 2005 January 26

ABSTRACT

We present high-resolution infrared spectra of V1647 Ori, the illuminating star of McNeil's Nebula, which reveal the presence of hot and cold gas-phase CO and ices of CO and H_2O. The emission lines of ^{12}CO (1–0), (2–1), and (3–2) likely originate from ~2500 K gas in an inner accretion disk region, where substantial clearing of dust has occurred. The width of the emission lines increases with increasing *J*-value, suggesting that the hottest CO gas we detect is located closest to the central star. The narrower widths of the low-*J* CO emission lines are indicative of more distant, cooler material in the inner disk. Superposed on the low-*J* emission lines are narrow ^{12}CO absorption components, which are typical of cold interstellar cloud material at a temperature of ~18 K. The very low column density and very cold temperature for the absorbing gas suggest that we are viewing the central star through intervening material within the L1630 cloud and that the disk is oriented nearly face-on. The Doppler shift of the cold CO is offset from the hot gas by 6 ± 2 km s^{-1}, so it is likely that the very cold CO originates in a foreground cloud rather than the circumstellar material surrounding V1647 Ori. Model fits to the strong H_2O and CO ice absorption bands are consistent with cold (<20 K) amorphous water ice ($\tau = 0.65$) and predominantly apolar CO ice ($\tau = 0.58$). The CO and H_2O ices are unprocessed (unannealed), similar to the ices in dense clouds.

Subject headings: infrared: ISM — ISM: individual (McNeil's Nebula) — reflection nebulae

1. INTRODUCTION

The near-infrared source V1647 Ori (2MASS J054613−000606), located in the Lynds 1630 cloud in Orion, was reported to have brightened enormously at visible wavelengths and to have revealed a cometary-shaped reflection nebula, which has been named after its discoverer Jay McNeil (McNeil et al. 2004). This rare event has sparked a flurry of observations spanning X-ray through radio wavelengths (Ábrahám et al. 2004; Andrews et al. 2004; Briceño et al. 2004; Kastner et al. 2004; Reipurth & Aspin 2004; Vacca et al. 2004). V1647 Ori appears to have brightened by as much as 5 mag in the *I* band over the course of about four months in late 2003 and early 2004 (Briceño et al. 2004). Subsequently, it was found to have gone through a similar brightening as recently as 1966 (Mallas & Kreimer 1978). Reipurth & Aspin (2004) show that the *J*, *H*, and *K′* bands have brightened by ~3 mag. Early reports suggested that the apparent brightening may have resulted from a rapid collapse of circumstellar disk material that fell onto the central star, similar in some ways to an FU Orionis or EX Lupi event (Briceño et al. 2004; Reipurth & Aspin 2004; Calvet et al. 1993). This proposed accretion event was not observed directly, and all observations subsequent to the brightening of V1647 Ori point to outflowing rather than inflowing material (e.g., Vacca et al. 2004).

The position of V1647 Ori coincides with that of an IRAS source (05436−0007) and a 1.3 mm source (LMZ 12), which Lis et al. (1999) suggested might be a Class 0 or somewhat more advanced protostar with an unresolved accretion disk. They further speculated that the faint *I*-band and near-infrared source now known as V1647 Ori had already dispersed the molecular gas in its immediate vicinity. Emission lines in optical as well as infrared spectra taken after the outburst of V1647 Ori have shown evidence for P Cygni structure due to a high-velocity wind (Reipurth & Aspin 2004; Vacca et al. 2004). The images of Reipurth & Aspin (2004) and the spectroscopy of Vacca et al. (2004), however, showed no evidence for shocked gas in H_2 (2.122 μm), which would be consistent with the absence of ambient cloud material in the close vicinity of V1647 Ori. Ábrahám et al. (2004), Andrews et al. (2004), and Vacca et al. (2004) suggested that V1647 Ori may be a Class I/Class II transitional object. From the spectral energy distribution, Ábrahám et al. (2004) derived a circumstellar mass of ~0.5 $M_\odot$, while Andrews et al. (2004) estimated the circumstellar mass to be an order of magnitude lower at ~0.05 $M_\odot$.

In this work, we present high-resolution infrared spectra of V1647 Ori, which reveal hot and cold gas-phase CO, and moderate-resolution spectra of ices of CO and H_2O. The analysis of the gas-phase CO lines is presented in § 3, and results for the ice analysis are presented in § 4. Section 5 presents a discussion of the results.

2. OBSERVATIONS

High-dispersion infrared observations (2–5 μm) of V1647 Ori were made on 2004 February 28 UT at the W. M. Keck Observatory on Mauna Kea, Hawaii, using the NIRSPEC spectrometer. Table 1 provides a list of the wavelengths observed. NIRSPEC provides a resolving power (RP) of 25,000 (McLean

[1] Current address: National Optical Astronomy Observatory, 950 North Cherry Avenue, Tucson, AZ 85719.

TABLE 1
NIRSPEC Settings

Setting	Order	Spectral Coverage (cm^{-1})
M-wide 1 (61.12, 37.05)[a]	14	1885–1855
	15	2019–1987
	16	2153–2118
M-wide 2 (66.4, 37.27)[a]	14	1857–1829
	15	1989–1960
	16	2120–2090
M-wide 3 (64.28, 36.70)[a]	15	1962–1935
	16	2091–2063
	17	2221–2191

[a] Echelle and cross disperser settings; the integration times for the three settings were 12, 16, and 12 minutes, respectively.

et al. 1998), which allows us to cleanly separate the fundamental (1–0) and excited (2–1) and (3–2) states of ^{12}CO and ^{13}CO as well as measure the CO ice feature. In the spectra, many CO rotational lines are detected in emission, and a few of them at low J-values are seen in absorption as well. The broad solid-state water and CO ice features within the wavelength range covered by our spectra are more readily analyzed from medium-resolution data. Vacca et al. (2004) have generously provided their SpeX observation for our analysis of the ice, which is discussed in § 4.

For each grating setting a series of flats and darks was taken to remove systematic effects. The images were cleaned of hot and dead pixels as well as cosmic-ray hits and were then resampled spectrally and spatially so that the resulting images placed spectral and spatial dimensions orthogonally, falling along rows and columns, respectively. Details of our reduction and analysis techniques can be found in Brittain et al. (2003, 2004). The observations began with the NIRSPEC entrance slit in a position angle of 15° and finished with a position angle of 45°. Flux calibration for the emission lines was achieved using the calibrated SpeX data

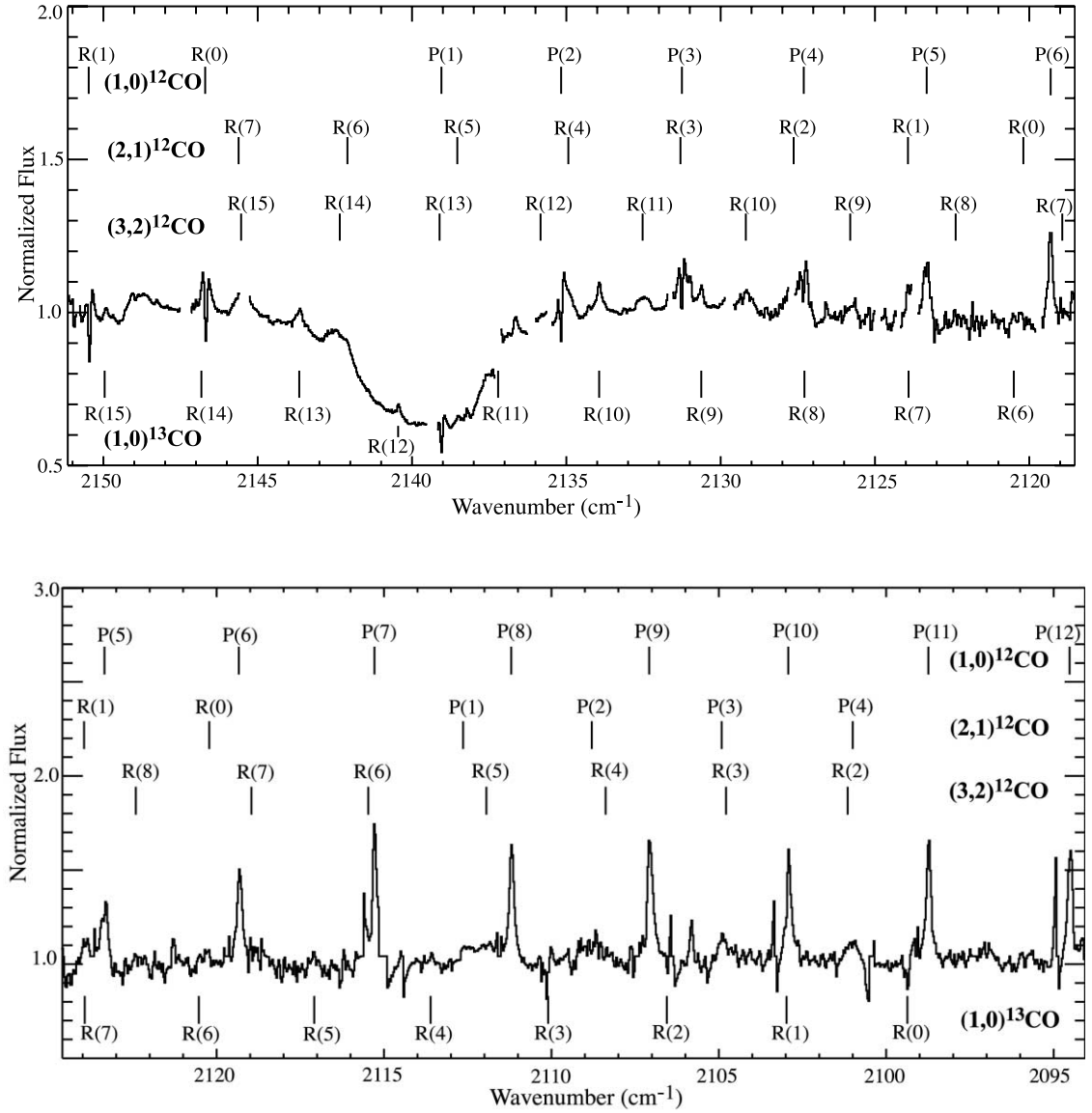

FIG. 1.—Sample spectra showing CO emission features for ^{12}CO (1–0), (2–1), and (3–2) and ^{13}CO. In the top panel the broad absorption feature at 2140 cm^{-1} is due to CO ice. The ^{12}CO emission lines have narrow absorption components superposed on the low-J lines only out to $P(4)$. The higher transitions of CO are detected to about $P(44)$; none of the high-J lines show signs of CO absorption. The atomic hydrogen line Pfβ was not detected at 2149 cm^{-1} (e.g., Simon et al. 2004). Our observations do not cover the Brα at 4.05 μm or the Brγ line at 2.17 μm.

TABLE 2
FUNDAMENTAL ^{12}CO (1, 0), ^{12}CO (2, 1), AND ^{13}CO (1, 0) EMISSION LINE PARAMETERS

Line ID	ν_{lab} (cm^{-1})	ν_{obs} (cm^{-1})	$\Delta\nu$ (cm^{-1})	v_{rad} (km s^{-1})	FWHM (km s^{-1})	Flux (10^{-17} W m^{-2})
Fundamental ^{12}CO (1, 0)						
R(21)	2218.75	2218.34	0.41	55	24 ± 2	9.68 ± 1.18
R(20)	2215.70	2215.29	0.41	56	24 ± 2	9.43 ± 0.72
R(18)	2209.51	2209.11	0.40	54	23 ± 2	7.03 ± 0.63
R(17)	2206.35	2205.98	0.37	51	23 ± 2	8.44 ± 0.68
R(15)	2199.93	2199.54	0.39	53	21 ± 2	7.79 ± 0.66
R(14)	2196.66	2196.27	0.40	55	23 ± 2	9.14 ± 0.71
R(13)	2193.36	2192.96	0.40	57	20 ± 2	7.35 ± 0.64
P(6)	2119.68	2119.29	0.40	56	25 ± 2	7.54 ± 0.68
P(7)	2115.63	2115.26	0.36	52	14 ± 2	7.16 ± 0.76
P(8)	2111.54	2111.16	0.38	54	22 ± 2	8.14 ± 0.70
P(9)	2107.42	2107.01	0.41	59	22 ± 2	7.94 ± 0.69
P(10)	2103.27	2102.89	0.38	55	22 ± 2	6.54 ± 0.63
P(11)	2099.08	2098.71	0.37	53	25 ± 2	8.85 ± 0.73
P(12)	2094.86	2094.49	0.38	54	20 ± 2	7.21 ± 0.67
P(14)	2086.32	2085.95	0.37	53	19 ± 2	6.91 ± 2.13
P(15)	2082.00	2081.65	0.36	51	21 ± 2	8.52 ± 2.37
P(17)	2073.26	2072.89	0.38	54	26 ± 2	8.08 ± 1.05
P(18)	2068.85	2068.49	0.36	52	20 ± 2	7.54 ± 1.16
P(19)	2064.40	2064.04	0.36	52	23 ± 2	7.80 ± 1.09
P(29)	2018.15	2017.78	0.37	55	28 ± 2	7.48 ± 0.98
P(30)	2013.35	2013.00	0.35	53	32 ± 2	6.43 ± 0.89
P(31)	2008.53	2008.13	0.40	59	37 ± 2	7.79 ± 1.00
P(32)	2003.67	2003.31	0.36	54	35 ± 2	5.92 ± 0.89
P(33)	1998.78	1998.39	0.39	59	36 ± 6	5.27 ± 0.87
P(36)	1983.94	1983.57	0.37	55	34 ± 3	4.61 ± 0.36
P(37)	1978.93	1978.56	0.36	55	36 ± 3	4.49 ± 0.74
P(38)	1973.89	1973.53	0.37	56	33 ± 3	4.07 ± 0.50
P(41)	1958.60	1958.25	0.35	53	39 ± 9	3.77 ± 0.96
P(42)	1953.45	1953.10	0.35	53	36 ± 9	3.33 ± 0.33
P(45)	1937.81	1937.47	0.35	54	39 ± 9	3.01 ± 0.31
^{12}CO (2, 1)						
P(7)	2089.39	2088.9	0.49	71	59 ± 17	5.24 ± 1.58
P(8)	2085.34	2084.98	0.36	52	52 ± 7	3.60 ± 0.62
P(24)	2016.03	2015.70	0.33	49	50 ± 2	4.48 ± 1.42
P(25)	2011.42	2011.01	0.41	61	47 ± 3	3.27 ± 0.25
P(26)	2006.78	2006.45	0.33	49	47 ± 3	2.98 ± 0.24
P(27)	2002.12	2001.77	0.35	52	56 ± 3	3.52 ± 0.24
P(28)	1997.42	1997.03	0.39	58	56 ± 3	3.66 ± 0.26
P(31)	1983.13	1982.72	0.41	62	56 ± 6	3.77 ± 0.43
P(32)	1978.31	1978.04	0.27	41	45 ± 10	4.22 ± 1.19
P(33)	1973.46	1973.09	0.37	56	49 ± 5	3.65 ± 0.37
^{13}CO (1, 0)						
R(15)	2150.34	2149.95	0.39	54	22 ± 3	0.96 ± 0.15
R(13)	2144.03	2143.66	0.37	52	24 ± 2	1.18 ± 0.14
R(12)	2140.83	2140.43	0.40	55	15 ± 2	0.96 ± 0.15
R(10)	2134.31	2133.93	0.38	54	18 ± 2	1.59 ± 0.17
R(9)	2131.00	2130.62	0.39	54	17 ± 1	1.36 ± 0.10
R(7)	2124.29	2123.91	0.38	53	17 ± 4	1.86 ± 0.47
P(7)	2069.66	2069.30	0.35	51	14 ± 2	1.80 ± 0.26

(Vacca et al. 2004). The emission lines, which span the fundamental vibrational band from $J' = 0$ to 44, are spectrally resolved at the 12 km s^{-1} resolution of NIRSPEC and appear symmetric in shape; they are not observed to be spatially extended along the slit.

Figure 1 presents two spectral extracts for the high-resolution infrared data from our 3–5 μm observations. The high-resolution M-band spectra of V1647 Ori reveal ^{12}CO gas in emission and absorption, emission lines from higher vibrational bands of ^{12}CO, and emission lines from ^{13}CO. The observed line positions, geocentric velocities, and the FWHM for each line are provided in Table 2.

3. GAS TOWARD V1647 ORI

3.1. CO *Emission*

The excitation plot for the CO emission lines, $(k/hcB)\ \ln\{F_J/[\tilde{\nu}^4(J' + J'' + 1)]\}$ versus $J'(J' + 1)$, is presented in Figure 2,

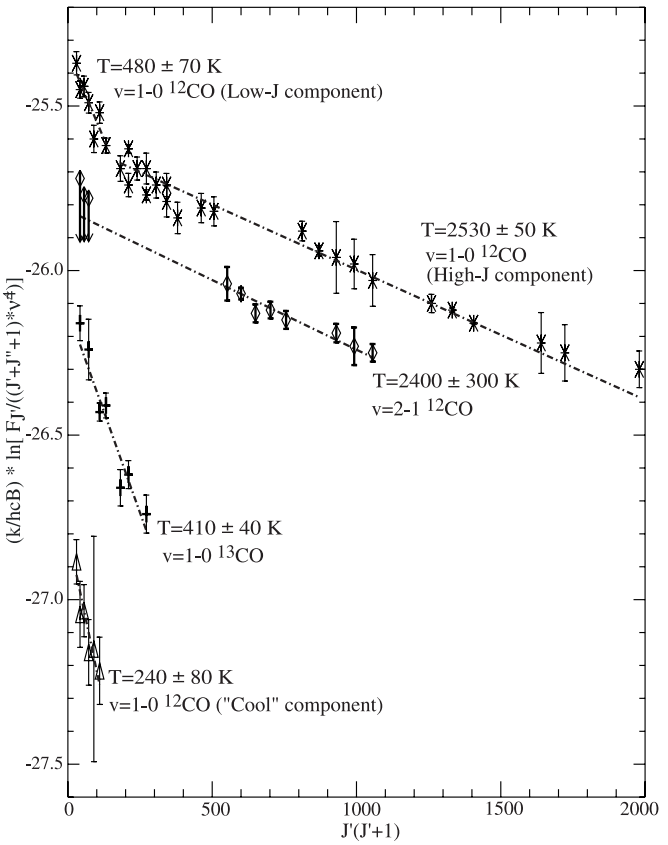

FIG. 2.—Rotational diagram of the CO emission lines for ^{12}CO (1–0) (hot and cold gas), ^{12}CO (2–1), and ^{13}CO (1–0). At the bottom of the figure, a corrected plot for the cooler ^{12}CO (1–0) gas is presented. A plot of $(k/hcB)\ \ln\{F_{J'}/[\tilde{\nu}^4(J' + J'' + 1)]\}$ vs. $J'(J' + 1)$ reveals a straight line for optically thin LTE gas, such that the negative reciprocal of the slope is the rotational temperature of the gas. The fit to the ^{12}CO (1–0) and ($v = 2-1$) high-J lines is linear and provides rotational temperatures of 2530 ± 50 and 2400 ± 300 K, respectively. The ^{13}CO (1–0) provides a rotational temperature of 410 ± 40 K. The linear fit to the low-J ^{12}CO (1–0) lines, with the flux contribution from the high-J lines removed, is presented at the bottom. These lines show the largest uncertainty after the warm CO component is subtracted.

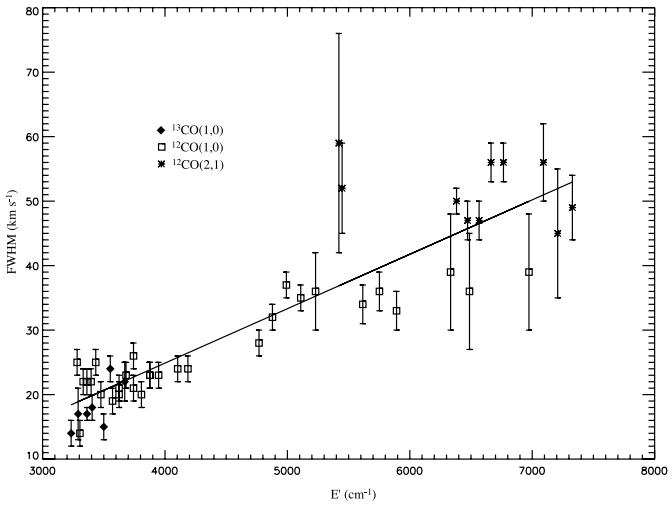

FIG. 3.—Width of the CO emission lines as a function of CO energy level. The open squares denote ^{12}CO (1, 0). The diamonds indicate ^{13}CO transitions, which are only detected for the low-J lines. The asterisks represent ^{12}CO (2, 1) lines, which are only detected for the high-J lines and probably originate nearest the star. The line widths increase with energy (and thus J-value), suggesting that the hotter material observed in the higher J lines is rotating faster, nearer the central star.

where the rotational temperature of the gas is given by the negative reciprocal of the slope. The excitation plot of the ^{12}CO (1, 0) transitions is not linear, which implies that either the gas is optically thick and/or the emission lines arise from gas having a range of temperatures (e.g., Brittain et al. 2003; Najita et al. 2003; González-Alfonso et al. 2002). In general, it is difficult to distinguish between these alternatives. However, we can exploit kinematic information to guide our analysis.

In particular, as shown in Figure 3, the width of the ^{12}CO fundamental emission lines is seen to increase with the upper-state energy level, E', which is proportional to $J'(J' + 1)$. If we assume that the line width is determined by Keplerian motion, the lower J lines ($J' < 25$), which are less broadened, must be formed farther from the star and consequently are dominated by cooler gas. The higher J lines are broader (have a larger Doppler width) and therefore must be dominated by material that is closer to the star.

The apparent trend in the CO line widths is consistent with the rotational temperatures we infer from the slopes of the regression lines shown in the excitation plots of Figure 2. The detection of the very high J lines indicates that some of the ^{12}CO gas we observe is remarkably hot. The rotational temperature in ^{12}CO (1, 0) determined from the slope of the fit to the $J = 12-44$ lines is 2530 ± 50 K. Similarly, the rotational temperature of the $v = 2-1$ lines ($J = 23-32$) is consistent with a value of 2400 ± 300 K. By comparison, the $v = 2-1$ lines in the CO spectrum of HL Tau yield a rotational temperature of 1500 K (Brittain et al. 2005), the emission from TW Hya gives ~400 K (Rettig et al. 2004b), and that of HD 141569 yields only ~200 K (Brittain et al. 2003). However, the high CO temperature for V1647 Ori that we derive here is not too surprising, given the detection of the $\Delta v = 2$ CO band heads at ~2.3 μm (Vacca et al. 2004), which require temperatures of at least 2000 K to be populated. The CO band head emission indicates the presence of hot, dense gas near the star. At this temperature, the lines are formed by collisional excitation with H and H_2, because neither UV nor IR pumping is capable of producing the observed rotational temperature distribution; essentially, the high-J transitions of ^{12}CO gas cannot be populated by photon pumping (Carr 1989; Scoville et al. 1980). Since dust sublimes at ~1500 K, it is clear that a substantial fraction of the hot CO emission originates in a portion of the inner disk that must be relatively free of dust.

On the other hand, the trend line for the ^{12}CO (1, 0) gas at low J-values [$R(1)$ through $P(4)$] suggests a cooler temperature of ~480 K; however, to determine the true rotational temperature of this "cool" component we must first remove the contribution from the hot gas to the flux of these low-J lines. The emission contributed by the hot gas to the flux of low-J lines was calculated by extrapolating from the high-J lines, which are obviously uncontaminated by the low-temperature gas. The corrected excitation plot of the low-J lines of ^{12}CO, shown in the lower portion of Figure 2, provides a temperature of 240 ± 80 K. This revised temperature is somewhat lower than our estimate of 410 ± 40 K for the ^{13}CO gas (Fig. 2), although the two are still consistent within the 3 σ errors and thus indicate a common origin. The considerably cooler temperature and relatively narrow line widths suggest that the low-J lines of ^{12}CO and ^{13}CO originate from a more distant, cooler gaseous disk component around V1647 Ori.

Since the emission lines are spectrally resolved, we can use their line profiles to make an estimate of the radial distribution of the gas (Najita et al. 2000, 2003). The velocity half-width at zero intensity (HWZI) of the broad emission lines at high J-values

TABLE 3
EQUIVALENT WIDTHS, OPACITY, AND COLUMN DENSITY FOR THE COLD CO GAS

Line ID	$\tilde{\nu}_{\rm rest}$ ($\rm cm^{-1}$)	$\tilde{\nu}_{\rm obs}$ ($\rm cm^{-1}$)	$\Delta\tilde{\nu}$ ($\rm cm^{-1}$)	$v_{\rm rad}$ ($\rm km\ s^{-1}$)	Equivalent Width (10^{-2} $\rm cm^{-1}$)	τ	$N_{J''}$[a] (10^{16} $\rm cm^{-2}$)
$R(1)$.....	2150.86	2150.51	−0.35	48	1.9 ± 0.1	8	1.25 ± 0.29
$R(0)$.....	2147.08	2146.73	−0.35	48	1.9 ± 0.1	8	0.84 ± 0.20
$P(1)$.....	2139.43	2139.08	−0.35	49	1.6 ± 0.1	4	1.33 ± 0.25
$P(2)$.....	2135.55	2135.21	−0.34	47	1.6 ± 0.1	4	1.12 ± 0.21
$P(3)$.....	2131.63	2131.30	−0.34	47	1.2 ± 0.1	2	0.52 ± 0.08
$P(4)$.....	2127.68	2127.34	−0.34	48	0.85 ± 0.1	1	0.28 ± 0.05
$P(5)$.....	2123.70	2123.36	−0.34	48	0.25 ± 0.1	0	0.06 ± 0.02

[a] The values for $N_{J''}$ result from $b = 0.85$.

corresponds to the radius of the gas at the inner edge of the warm emitting region, and the velocity half-width at half-maximum (HWHM) corresponds to half the radius of the upper limit on the outer edge of the emitting region (Najita et al. 2003). To construct an average line profile for the high-J lines, we used the ^{12}CO high-J fundamental and $v = 2$–1 lines, as these lines are minimally affected by telluric absorption. The HWZI of the average profile corresponds to $v \sin i = 90 \pm 5$ km s^{-1}; thus, the radius of the inner edge of the hot CO emitting region is $R_{\rm inner} = 0.11 M_{\rm star} \sin^2 i$ AU.[2] The HWHM of the average profile is 26 ± 5 km s^{-1}, which implies an outer radius of $2.6 M_{\rm star} \sin^2 i$ AU for the region. Similarly, for the relatively narrow low-J lines of ^{13}CO, the HWZI = 25 and HWHM = 13 km s^{-1} of the average profile imply $1.4 M_{\rm star} \sin^2 i$ AU for the inner radius and $11 M_{\rm star} \sin^2 i$ AU for the outer radius of the region that gives rise to the cooler gas we observe. Although the rotational temperatures are suggestive of two distinct populations of gas, the line profiles indicate that there is a substantial degree of radial overlap.

3.2. CO *Absorption*

The low-J emission lines of ^{12}CO (1–0) have absorption features superimposed on them (Fig. 1). We have measured equivalent widths of absorption-line profiles from the spectra in two ways: first by summing the absorption area, and second via Gaussian fits to the line profiles. Uncertainties were estimated from the mean deviations from the Gaussian fits and by the formal uncertainty in the fitted continuum level. The equivalent width, column density, and optical depth of each line are presented in Table 3.

Since the $R(1)$ line and the $P(1)$ line do not yield similar column densities, these lines are optically thick. To infer the proper column density and rotational temperature of the gas, we perform a curve-of-growth analysis on the absorption lines (Brittain et al. 2005; Kulesa 2002).

[2] For material in a circular, Keplerian orbit $R = 900 M_{\rm star}/v^2$, where R is the radius in AU, v is the velocity in km s^{-1}, and $M_{\rm star}$ is the mass of the star in solar masses.

TABLE 4
PARAMETERS FOR DIFFERENT INTRINSIC DOPPLER WIDTHS

b ($\rm km\ s^{-1}$)	$N(R(1))/N(P(1))$	$T_{\rm rot}$ (K)	$N_{\rm total}$ (10^{16} $\rm cm^{-2}$)	χ^2
0.60.....	2.0 ± 1.0	12.3 ± 0.8	15.4 ± 3.5	1.56
0.70.....	1.4 ± 0.6	14.8 ± 0.9	7.0 ± 1.2	1.21
0.80.....	1.0 ± 0.4	17 ± 1	4.5 ± 0.6	0.99
0.90.....	0.9 ± 0.2	18 ± 1	3.5 ± 0.4	1.01
1.0.....	0.8 ± 0.2	20 ± 1	3.0 ± 0.3	1.22

The fact that the $R(1)$ line and the $P(1)$ line probe the same lower state allows us to estimate the intrinsic Doppler width, $b = \rm FWHM/1.665$, of the absorption lines (Brittain et al. 2005). For $b = 0.7$–1.0 km s^{-1}, the R-branch and P-branch column densities are in agreement (Table 4); however, this is only one set of lines with a substantial uncertainty. We further constrain b by selecting the value that best linearizes an excitation diagram for the absorption lines. By minimizing χ^2, we find that $0.8 \leq b \leq 0.9$ km s^{-1} (Table 4). Thus, the resulting total column density of cold ^{12}CO is $(4 \pm 1) \times 10^{16}$ cm^{-2}, and the rotational temperature is 18 ± 1 K (Fig. 4). The observed Doppler shift of the cold CO absorption lines is 48 ± 1 km s^{-1}, whereas the Doppler shift of the hot emission lines is 54 ± 2 km s^{-1}. When corrected for the Earth's motion, the average heliocentric radial velocity is $v_{\rm rad} = 23 \pm 1$ km s^{-1} for the absorption lines and 29 ± 2 km s^{-1} for the CO emission lines. The relative velocity difference, 6 ± 2 km s^{-1}, implies that the cold gas is foreground material rather than circumstellar.

In the next section we show that at this cold temperature, a significant portion of the CO along the line of sight to V1647 Ori is bound up in ice.

4. H_2O AND CO ICE TOWARD V1647 ORI

Vacca et al. (2004) obtained a medium-resolution (RP $\sim$ 2500) spectrum of V1647 Ori with the SpeX facility spectrograph at the NASA Infrared Telescope Facility (IRTF; 2004

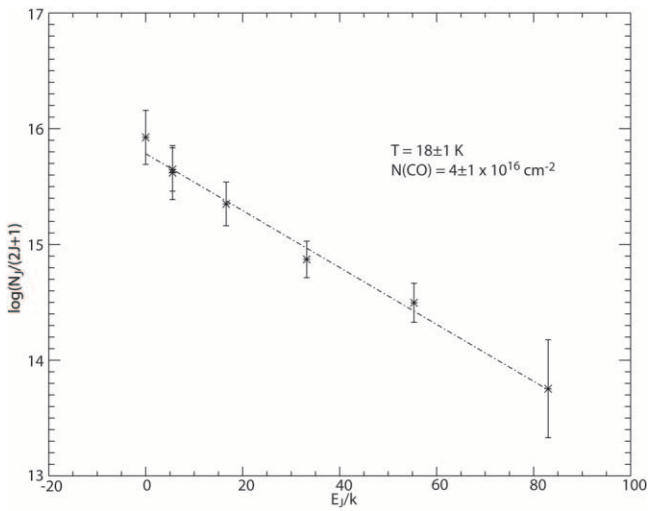

FIG. 4.—Rotational temperature diagram of the cold ^{12}CO (1–0) absorption component. The linear fit to the plot (using $b = 0.85$) indicates that the optical depth effects have been corrected. The inverse slope of the plot is proportional to the rotational temperature (18 ± 1 K).

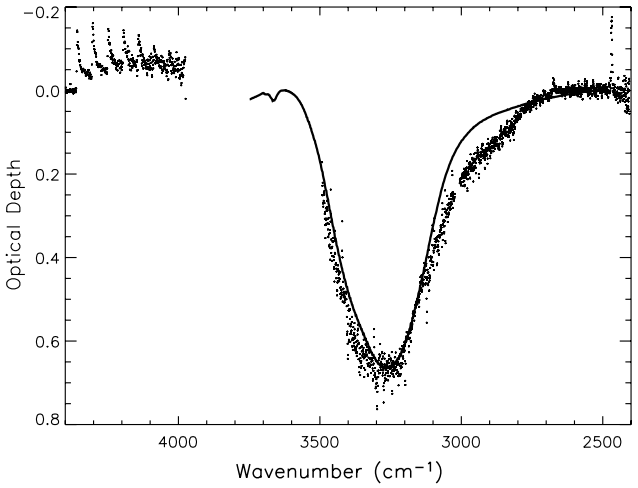

FIG. 5*a*

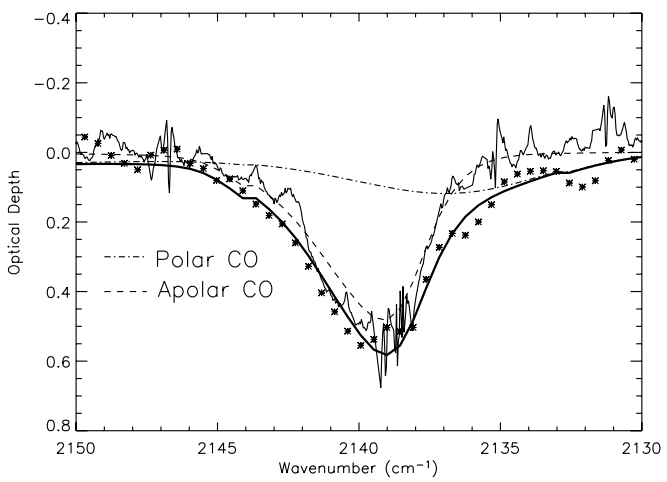

FIG. 5*b*

FIG. 5.—(*a*) Optical depth spectrum for H_2O ice. The solid black line is the best fit to the data and corresponds to pure water at 10 K that has undergone scattering. The best model corresponds to a maximum ice mantle thickness of 0.35 μm. (*b*) Optical depth spectrum for CO ice. The data points defined by asterisks are the SpeX data (courtesy of Vacca et al. 2004), and the narrow solid line data are from NIRSPEC. The dashed line corresponds to the apolar component ($H_2O:CO:O_2$, 1 : 20 : 60 at 30 K), and the dot-dashed line corresponds to the polar component ($H_2O:CO_2:CO$, 100 : 20 : 3 at 20 K). The smooth solid black line is the best fit to the data, corresponding to the sum of the apolar and polar contributions. We fit to the SpeX data because the continuum was better defined. The ice absorption features indicate that the underlying star is embedded in the Orion L1630 cloud.

February 27 UT) and have kindly provided the spectrum to us for the analysis of the O—H and C≡O stretch modes of water and CO ice at 3.05 and 4.67 μm, respectively. The CO ice band was also observed with NIRSPEC on the following night at Keck (see Fig. 1). The H_2O and CO ice bands are presented in Figures 5*a* and 5*b*, respectively.

The optical depths of the ice features were determined by fitting a polynomial to continuum points on either side of the ice absorption. To analyze these features, we used laboratory data from the Leiden Molecular Astrophysics group[3] and Hudgins et al. (1993) and made a least χ^2 fit to the optical depth spectrum of each ice feature simultaneously with two laboratory spectra. In the case of H_2O, a combination of both warm and cold ice components was investigated for cases with and without scattering. The scattering model used was based on the core-mantle Mie scattering code developed by Bohren & Huffman (1983) and is discussed in detail in Chiar et al. (2002). In this model, we assume equal numbers of silicate and graphite grains with a size distribution $n(a_c)\,da_c \propto a_c^{-3.5}\,da_c$, where a_c is the core size, ranging over $0.005 < a_c < 0.25$ μm. This model should be a reasonable first approximation to the grain size distribution in dense clouds (e.g., Smith et al. 1993; Whittet et al. 1996; Holbrook & Temi 1998). Our model also incorporates a mantle thickness distribution, as discussed by Smith et al. (1993) and Chiar et al. (2002).

Our best laboratory fit to the H_2O ice band toward V1647 Ori (see Fig. 5*a*) is for a scattering model using cold ($\sim$10 K) amorphous (unprocessed) ice on silicate and graphite grain cores having a maximum mantle thickness of 0.35 μm. A similar water ice band is seen toward Elias 16, a K giant located behind the Taurus dark cloud in a region believed to be devoid of star formation (Smith et al. 1993; Gibb et al. 2004). The column density of H_2O ice was determined using $N = \int \tau\, d\lambda / A$, where A is the band strength determined in the laboratory. For water, we use $A = 20 \times 10^{-17}$ cm molecule^{-1} (d'Hendecourt & Allamandola 1986), giving $N(H_2O) = (1.2 \pm 0.1) \times 10^{18}$ cm^{-2}.

For the 4.67 μm C ≡ O stretch feature of CO ice, we simultaneously fit combinations of both apolar and polar CO as well as combinations of pure CO with polar and apolar mixes. The best laboratory fits are shown in Figure 5*b*. The dot-dashed line shows the polar ice contribution, the dashed line shows the apolar ice contribution, and the bold line shows the total CO ice laboratory fit. The profile is clearly dominated by cold (<20 K) apolar CO mixtures in which CO is in an ice matrix with such species as CO_2, O_2, and possibly a very small amount of water. The band strength of CO was assumed to be 1.1×10^{-17} cm molecule^{-1} (Gerakines et al. 1995), resulting in $N(CO) = (2.4 \pm 0.2) \times 10^{17}$ cm^{-2}, of which up to 5% may be due to CO in a polar (water-rich) mixture. Comparing this to water, we determine $N(CO)/N(H_2O) = 0.20 \pm 0.02$. This high abundance of CO is consistent with that seen toward quiescent dark clouds and low-mass star formation regions (Gibb et al. 2004 and references therein). Coupled with the low temperatures and profile shapes, we conclude that the CO ice along the line of sight toward V1647 Ori is predominately in an apolar matrix ice and has not been thermally processed.

We also note the results of Andrews et al. (2004) for V1647 Ori, where they report no evidence for the 9.7 μm silicate feature in either absorption or emission. While there are other young stars without silicate features (see, e.g., Hanner et al. 1998; Kessler-Silacci et al. 2005), these objects also lack ice absorption. Ices need a particle on which to condense, thought to be primarily cold silicate dust grains. Near young stellar objects, the silicate feature is often dominated by an emission component (Bowey et al. 2003), and it is possible to have ice absorption toward these objects as the ice is condensed on the cold silicate grains along the line of sight between us and the hot young star. To have a source with significant ice absorption and no evidence of silicates is perplexing. Further study of the solid-state component toward V1647 Ori and other young stars is necessary to resolve this mystery.

5. DISCUSSION

The extinction toward V1647 Ori has been estimated to be $A_V = 8$–14 mag (Briceño et al. 2004; Ábrahám et al. 2004; Andrews et al. 2004; Vacca et al. 2004). Given this extinction, the column of intervening cold CO gas that we measure,

[3] See http://www.strw.leidenuniv.nl/~lab.

$N(\mathrm{CO}) = (4 \pm 1) \times 10^{16}$ cm^{-2}, is too small to be explained with abundances typical of dark clouds, where $\mathrm{CO/H_2} = 1.5 \times 10^{-4}$ (Kulesa 2002; Kulesa & Black 2003). The presence of significant CO ice in the M-band spectrum indicates that gas depletion onto dust grains dominates; indeed, the abundance of solid CO exceeds that of gas-phase CO by a factor of 6.

Models describing the photodissociation of CO and H_2 as a function of depth into a cloud can be used to illustrate the abundance gradients at the surface of clouds exposed to an external radiation field. For example, if the intervening material has a density $n_{\mathrm{H}} \sim 10^4$ cm^{-3}, is illuminated by a modest radiation field ($I_{\mathrm{UV}} = 1$–10),[4] and is composed of "dark cloud" dust grains, then a total CO column of $\sim 3 \times 10^{17}$ cm^{-2} implies a depth of $N(\mathrm{H_2}) = 7.2 \times 10^{21}$ cm^{-2}, $N(\mathrm{H}) = 3.3 \times 10^{20}$ cm^{-2}, and $A_V \sim 9$ mag (Kulesa 2002; Brittain et al. 2005). These results have only moderate sensitivity to cloud parameters; application of "diffuse cloud" grains reduces A_V to 6, whereas an increase in radiation field ($I_{\mathrm{UV}} = 10^2$–10^3) requires more extinction ($A_V \sim 11$) to shield the same column of CO. Standard cloud models are therefore able to unify the observed extinction toward V1647 Ori and the low abundance of CO.[5]

Does the CO absorption originate from material in a flared disk, as may be typical of many young stars, or from an intervening interstellar dust cloud? As an interesting comparison, V1647 Ori has a column density of absorbing CO gas that is relatively small (0.5%) compared to HL Tau (Brittain et al. 2005; Rettig et al. 2004a). Both objects are similar Class I/Class II transitional stars with about the same circumstellar mass $\sim 0.05\ M_\odot$ (see Sargent & Beckwith 1991 [much larger]; Lay et al. 1994; Mundy et al. 1996; Wilner et al. 1996; Ábrahám et al. 2004; Andrews et al. 2004). HL Tau has an inclination $\sim 67^\circ$ (Lucas et al. 2004) and an $A_V \sim 24$ (Close et al. 1997). Its high gas-phase CO column density $N(\mathrm{CO}) = 7.5 \times 10^{18}$ and temperature ($\sim$100 K) indicate an origin in the flared disk (Brittain et al. 2005). For V1647 Ori, the much lower extinction and much smaller N(CO) suggest that we are viewing a very nearly face-on disk. Furthermore, the Doppler shift of the cold CO is offset from the hot gas by 6 ± 2 km s^{-1} (see Tables 2 and 3), so it is likely that the very cold CO (18 K) originates in a foreground cloud rather than the circumstellar material surrounding V1647 Ori.

The absorption-line results imply that we are looking through a cold dense cloud in front of a young protostar, and the low column density of CO in absorption from the disk implies an inclination $<30^\circ$. This orientation is in agreement with Andrews et al. (2004), who use a nearly face-on disk to explain the nondetection of the silicate feature. They suggest that the effects of emission from the disk and absorption from intervening cloud material cancel. However, if we were looking through even part of a massive ($0.05\ M_\odot$) flared disk, the N(CO), extinction, and CO absorption temperature would be much higher than observed, and the ice would be annealed.

The high- and low-J emission lines of ^{12}CO and ^{13}CO suggest that the CO gas around V1647 Ori consists of a very hot ($\sim$2500 K) component near the central star and a more distant, cooler disk component, which is only a few hundred K. For illustration, if we assume an inclination of 30° and a stellar mass of $1\ M_\odot$, the hot CO emission would have an inner radius of $\sim$0.03 AU and extend to $\sim$0.7 AU (see § 3). The inner radius is similar to the corotation radius of classical T Tauri stars for which the inclination has been measured (Najita et al. 2003). Applying the same parameters to calculate the spatial extent of the low-J lines of ^{13}CO emission, we find that the inner radius is $\sim$0.4 AU and it extends to at least 2.8 AU.

Because the temperature of the hot gas ($\sim$2500 K) exceeds the dust sublimation temperature, the most likely scenario for the hot broad emission lines suggests a dust gap that extends from a few solar radii out to a radius of perhaps 0.7 AU. This outer radius may be a bit overestimated if the gas is pressure supported and not in Keplerian motion with the central disk. For the cooler (200–400 K) gas component, the emission lines may originate from a region in the disk midplane that is optically thin (see Najita et al. 2000) out to nearly 3 AU. Alternatively, these cooler emission lines could originate from a region in the vertically extended outer disk atmosphere that is warmer than an optically thick inner disk (e.g., Kamp & Dullemond 2004; Glassgold et al. 2004; Gorti & Hollenbach 2004). Determining whether this last alternative can account for the overlapping emission regions (see § 3.1), as arising from different optical depths seen radially along the disk, will require observations of other species such as OH and H_2O that will probe different temperatures and densities in the disk.

Since V1647 Ori and HL Tau are likely in similar evolutionary states (both are Class I/Class II transitional sources), it is interesting to note that Lin et al. (1994) have suggested that HL Tau is an FU Orionis star in quiescence. For HL Tau, Brittain et al. (2005) have shown that the CO emitting region extends to only $\sim$0.3 AU, in contrast to V1647, where the gas emitting region likely extends much farther. Perhaps the disk of HL Tau was previously in a state similar to V1647 Ori and has since partially refilled the inner disk.

There are various disk thermal instability models that have been used to explain the rapid accretion rates in FU Orionis type stars (Bonnell & Bastien 1992; Armitage et al. 2001; Bell & Lin 1994; Petrov & Herbig 1992), but none have satisfactorily accounted for the initial rise times and duration of the outbursts. Recently, Lodato & Clarke (2004) demonstrated that a thermal instability in the disk might be the result of a mass build-up at a radius outward of a 10–15 Jovian mass planet. In this scenario the build-up continues until the critical value for thermal instability is reached, which leads to a reasonable depiction of the observed accretion rates and brightness rise times. The rise time is dependent on the planetary mass, and the duration of the event is dependent on the propagation radius.

If an analogous phenomenon is now occurring for V1647 Ori, quantifiable effects of a refilling of the inner disk region ($R < 2.8$ AU) should be measurable. As the inner disk is refilled with dust, the CO emission-line profiles should broaden and reveal a smaller emitting region. Since this star has recently brightened and high-resolution spectra are sensitive to small changes in the CO emission-line profiles (on the order of a few km s^{-1}), the effects should be observable.

6. CONCLUSION

The high-resolution CO emission spectra of V1647 Ori show many similarities with young T Tauri stars (Najita et al. 2003). The widths of the broad ^{12}CO (1–0), (2–1), and (3–2) emission lines increase with increasing J-value, suggesting that the hot CO gas ($\sim$2500 K) we are detecting is close to the central star. The less broadened (lower J) ^{12}CO and ^{13}CO lines are indicative of more distant and cooler ($\sim$200–400 K) disk material. If the recent outburst was tied to a clearing of the inner disk, future observations can be used to quantify the distribution and temperature of the CO emission lines as the gap refills with gas and dust in preparation for the next outburst.

[4] Note that $I_{\mathrm{UV}} = 1$ corresponds to an integrated intensity of 912–1130 Å photons of 4.76×10^{-5} ergs s^{-1} cm^{-2} sr^{-1}.

[5] If $A_V = 10$, the resulting $A_M = 0.03$ will not appreciably affect the calculation of the CO column density or the rotational temperature, as the effect of extinction is smaller than our uncertainty in the flux of the lines.

Superposed on the low-J broad emission features are narrow ^{12}CO absorption components typical of cold interstellar cloud material ($\sim$20 K). The absorption-line results suggest that we are viewing the central star through the cold intervening material from the L1630 cloud along our line of sight. Model fits to the prominent H_2O and CO ice profiles are consistent with cold ($<$20 K) amorphous water ice ($\tau = 0.65$) and predominantly apolar CO ice ($\tau = 0.58$). The CO and H_2O ices are unprocessed (unannealed), similar to ices found in dense clouds. The implication is that the very cold CO absorption as well as the ices detected along the line of sight are not directly associated with the star or disk of V1647 Ori.

T. W. R., E. L. G., and S. D. B. were supported by NSF grant AST 02-05881. The data presented herein were obtained at the W. M. Keck Observatory, which is operated as a scientific partnership among the California Institute of Technology, the University of California, and the National Aeronautics and Space Administration. The Observatory was made possible by the generous financial support of the W. M. Keck Foundation. We would like to thank the anonymous reviewer for many helpful suggestions. We especially thank W. D. Vacca and M. C. Cushing for generously providing us with the SpeX data from the NASA IRTF and also W. D. Vacca for his comments on the draft.

REFERENCES

Ábrahám, P., Kóspál, Á., Csizmadia, Sz., Moór, A., Kun, M., & Stringfellow, G. 2004, A&A, 419, L39
Andrews, S. M., Rothberg, B., & Simon, T. 2004, ApJ, 610, L45
Armitage, P. J., Livio, M., & Pringle, J. E. 2001, MNRAS, 324, 705
Bell, K. R., & Lin, D. N. C. 1994, ApJ, 427, 987
Bohren, C. F., & Huffman, D. R. 1983, Absorption and Scattering of Light by Small Particles (New York: Wiley)
Bonnell, I., & Bastien, P. 1992, ApJ, 401, L31
Bowey, J. E., Adamson, A. J., & Yates, J. A. 2003, MNRAS, 340, 1173
Briceño, C., Vivas, J., Hernandez, J., Calvet, N., Hartmann, L., Megeath, T., Berlind, P., Calkins, M., & Hoyer, S. 2004, ApJ, 606, L123
Brittain, S. D., Rettig, T. W., Simon, T., & Kulesa, C. 2005, ApJ, 625, in press
Brittain, S. D., Rettig, T. W., Simon, T., Kulesa, C., DiSanti, M. A., & Dello Russo, N. 2003, ApJ, 588, 535
Brittain, S. D., Simon, T., Kulesa, C., & Rettig, T. W. 2004, ApJ, 606, 911
Calvet, N., Hartmann, L., & Kenyon, S. J. 1993, ApJ, 402, 623
Carr, J. S. 1989, ApJ, 345, 522
Chiar, J. E., Adamson, A. J., Pendleton, Y. J., Whittet, D. C. B., Caldwell, D. A., & Gibb, E. L. 2002, ApJ, 570, 198
Close, L. M., Roddier, F., Northcott, M. J., Roddier, C., & Graves, J. E. 1997, ApJ, 478, 766
d'Hendecourt, L. B., & Allamandola, L. J. 1986, A&AS, 64, 453
Gerakines, P. A., Schutte, W. A., Greenbert, J. M., & van Dishoeck, E. F. 1995, A&A, 296, 810
Gibb, E. L., Whittet, D. C. B., Boogert, A. C. A., & Tielens, A. G. G. M. 2004, ApJS, 151, 35
Glassgold, A. E., Najita, J., & Igea, J. 2004, ApJ, 615, 972
González-Alfonso, E., Wright, C. M., Cernicharo, J., Rosenthal, D., Boonman, A. M. S., & van Dishoeck, E. F. 2002, A&A, 386, 1074
Gorti, U., & Hollenbach, D. 2004, ApJ, 613, 424
Hanner, M. S., Brooke, T. Y., & Tokunaga, A. T. 1998, ApJ, 502, 871
Holbrook, J. C., & Temi, P. 1998, ApJ, 496, 280
Hudgins, D. M., Sandford, S. A., Allamandola, L. J., & Tielens, A. G. G. M. 1993, ApJS, 86, 713
Kamp, I., & Dullemond, C. P. 2004, ApJ, 615, 991
Kastner, J. H., et al. 2004, Nature, 430, 429
Kessler-Silacci, J. E., Hillenbrand, L. A., Blake, G. A., & Meyer, M. R. 2005, ApJ, 622, 404
Kulesa, C. A. 2002, Ph.D. thesis, Univ. Arizona
Kulesa, C. A., & Black, J. H. 2003, in Chemistry as a Diagnostic of Star Formation, ed. C. L. Curry & M. Fich (Ottawa: NRC Press), 60
Lay, O. P., Carlstrom, J. E., Hills, R. E., & Phillips, T. G. 1994, ApJ, 434, L75
Lin, D. N. C., Hayashi, M., Bell, K. R., & Ohashi, N. 1994, ApJ, 435, 821
Lis, D. C., Menten, M., & Zylka, R. 1999, ApJ, 527, 856
Lodato, G., & Clarke, C. J. 2004, MNRAS, 353, 841
Lucas, P. W., et al. 2004, MNRAS, 352, 1347
Mallas, J. H., & Kreimer, E. 1978, The Messier Album (Cambridge: Sky Publ. Corp.)
McLean, I. S., et al. 1998, Proc. SPIE, 3354, 566
McNeil, J. W., Reipurth, B., & Meech, K. 2004, IAU Circ., 8284, 1
Mundy, L. G., et al. 1996, ApJ, 464, L169
Najita, J. R., Carr, J. S., & Mathieu, R. D. 2003, ApJ, 589, 931
Najita, J. R., Edwards, S., Basri, G., & Carr, J. 2000, in Protostars and Planets IV, ed. V. Mannings, A. P. Boss, & S. S. Russell (Tucson: Univ. Arizona Press), 457
Petrov, P. P., & Herbig, G. H. 1992, ApJ, 392, 209
Reipurth, B., & Aspin, C. 2004, ApJ, 606, L119
Rettig, T. W., Brittain, S., Simon, T., Kulsea, C., & Haywood, J. 2004a, in AIP Conf. Proc. 713, The Search for Other Worlds, ed. S. Holt & D. Deming (New York: AIP), 107
Rettig, T. W., Haywood, J., Simon, T., Brittain, S. D., & Gibb, E. 2004b, ApJ, 616, L163
Sargent, A. I., & Beckwith, S. V. W. 1991, ApJ, 382, L31
Scoville, N. Z., Krotkov, R., & Wang, D. 1980, ApJ, 240, 929
Simon, T., Brittain, S. D., Gibb, E. L., & Rettig, T. W. 2004, IAU Circ., 8303, 2
Smith, R. G., Sellgren, K., & Brooke, T. Y. 1993, MNRAS, 263, 749
Vacca, W. D., Cushing, M. C., & Simon, T. 2004, ApJ, 609, L29
Whittet, D. C. B., et al. 1996, ApJ, 458, 363
Wilner, D. J., Ho, P. T. P., & Rodriguez, L. F. 1996, ApJ, 470, L117